Influence of Boron on Texture and Segregation in Modified 9Cr-2W Steel after Cold Pilgering Process

Hyeong Min Heo [a,b], Jun Hwan Kim[b], Sung Ho Kim [b], Jong Ryoul Kim[a]*

[a]Department of Materials Engineering, Hanyang University, 55, Hanyangdaehak-ro, Sangnok-gu, Ansan-si, Republic of Korea

[b]Advanced Fuel Development Division, KAERI, 989-111, Daedeok-daero, Yuseong-gu, Daejeon, 305-353, Republic of Korea

[*]Corresponding author: jina@hanyang.ac.kr

1. Introduction

As a future nuclear energy system, the SFR (sodium-cooled fast reactor) is economic, stable and reliable because it uses high-speed neutrons and liquid sodium as a coolant [1,2]. The main components of the SFR are the nuclear fuel assemblies and nuclear fuel cladding. The nuclear fuel cladding component determines the stability of the nuclear reactor, and its function is to hold metal fuels and fission materials while efficiently transferring fission energy. Because irradiation with fast neutrons generates thermal creep and swelling, the nuclear fuel cladding tubes must provide excellent swelling resistance, creep resistance and high-temperature strength for long periods of time. To meet these requirements, the nuclear fuel cladding of a sodium-cooled fast reactor is typically 9-12% Cr FM (ferritic martensitic) steel. This ensures outstanding thermal conductivity, a low thermal expansion coefficient, and high resistance to void swelling [2]. In order to develop an SFR fuel cladding material with excellent high-temperature creep characteristics, research is underway to improve the stability of the microstructure by adding precipitation-strengthening elements (C, N, V, Nb and Ta) and solid-solution strengthening alloying elements (Cr, W, Mo and B). Subsequently, alloys with high creep strength were selected by adjusting the contents of boron and nitrogen and were fabricated as nuclear fuel cladding components [3].

Pilgering is a metal-working process for reducing the dimensions of a metal tube. The two key components of a pilgering press (or mil) are a conical mandrel, which fits inside the tube and ring dies which roll over the outside of the tube. This process reduces the diameter of the tube to the size of the mandrel and, at the same time, reduces the wall thickness of the tube from the action of the dies rolling over the outside of the tube along the mandrel.

Boron is known as an element that inhibits the growth of $M_{23}C_6$ and improves the stability of microstructures [4]. FM steel with 9-12% Cr was used in a SIMS analysis of the distribution of boron at the grain boundaries arising due to the effects of normalizing and tempering processes. But failure occurred under conditions including normalized tube and tempered after normalizing tube when drawing process. This

phenomenon is considered to be caused by the normalizing heat treatment which may take place fracture during the drawing process.

In this study, a heat treatment process after a pilgering process led to a failure during the drawing step. In order to optimize the manufacturing process for fuel cladding tubes, changes of the microstructure, texture were investigated with different heat treatment conditions.

2. Methods and result

2.1 Materials and fabrication process

The chemical composition of the modified 9Cr-2W steel used here is shown in Table 1. The modified 9Cr-2W steel was prepared by a vacuum induction melting (VIM) process. The prepared ingot was subjected to forging to break up the segregation in the cast microstructure which occurred during the VIM process after heating to 1170°C. In order to soften the martensitic structure produced during the forging process, a heat treatment was conducted. A hot extruded pipe with an outer diameter of 46 mm, a thickness of 3.5 mm and a length of 6100 mm was manufactured. It was tempered to soften the deformed structure created during the extrusion process. A pilgered tube with an outer diameter of 25.4 mm and a thickness of 1.65 mm was prepared through a pilgering process. The heat treatment used had four different conditions. These were the pilgered condition (no heat treatment), the normalized condition (1040°C/4 min/air cooled), the tempered condition (760°C/6 min/air cooled), and the N&T condition (760°C/6 min/air cooled after 1040°C/4 min/air cooled).

Table 1 Chemical composition of steels (wt%).

	C	Cr	Mo	B	N	Ta	W
Alloy B	0.07	8.89	0.44	0.013	0.020	0.04	1.93

2.2 Observation of the microstructure

Specimens for the microstructural observations were prepared by grinding and polishing (up to 0.25 m diamond suspension), with a subsequent etching step

(95 ml water + 3 ml nitric acid + 2 ml fluoric acid) applied to all samples. The microstructures after the four heat treatment conditions were investigated EBSD (electron backscattered diffraction) after a metallographic sample preparation step. An additional one-hour polishing step with a 0.04 μm colloidal silica suspension was performed afterwards. EBSD patterns were acquired on a Su5000 instrument equipped with a Hikari detector operated with EDAX-TSL OIM DATA Collection software. SIMS imaging with a CAMECA Nano-SIMS device was used to observe the boron segregation at the grain boundaries. The nano-SIMS specimens were prepared using a procedure identical to that above and were analyzed. Nano-SIMS measurements with statistical errors of less than 0.2% were taken using a CS^+ gun beam with an 80-nm diameter and impact energy of 16 keV and 0.35 pA. Prior to the acquisition of the distribution maps, the concentration depth profiles of $11B^+$, $12C^-$ and $16Cr^+$ were determined by nano-SMS in an area of 10 x 10 μm^2 and it detected $11B16O2^-$, $12C^-$ and $52Cr16O^-$ ions and received images of the boron, carbon, chromium and tungsten. This analysis was carried out at the Busan center of the Korea Basic Science Institute (KBSI). The nano-SIMS specimens were observed by means of EBSD at the same regions.

2.3 Comparison of the segregation behavior of boron with different intermediate heat treatment conditions

In order to compare the segregation of boron at the grain boundary in the tempered condition, normalized condition and N&T condition, the heat treatment conditions were examined using Nano-SIMS. Nano-SIMS images and the distribution map of boron, carbon and chromium in the area marked by the arrow with the different intermediate heat treatment conditions are presented in Fig. 1. The normalized condition shows segregated boron and carbon at the grain boundaries, while chromium is distributed at a small amount in the grain interior regions and at the grain boundaries. The tempered condition and the N & T condition show that the distributions of boron and carbon coincided with the distribution of chromium. On the other hand, W is distributed at a small amount in the grain boundary and grain interior regardless of heat treatment. The segregation of boron occurred at the grain boundary in all intermediate conditions. The difference in the segregation behavior between the normalized condition and the tempered condition can be explained by the boundary characteristics and precipitation.

2.4 Texture

Crystallographic textures that form during the various heat treatment processes were determined by an EBSD analysis. Orientation distribution functions (ODF) $f(g)$

were calculated by the harmonic series expansion method according to Bunge (l =22) from their incomplete pole figure {110}, {200} and {211} [4]. The orientation g was expressed in the form of a triple Euler angle (φ_1, Φ, φ_2).
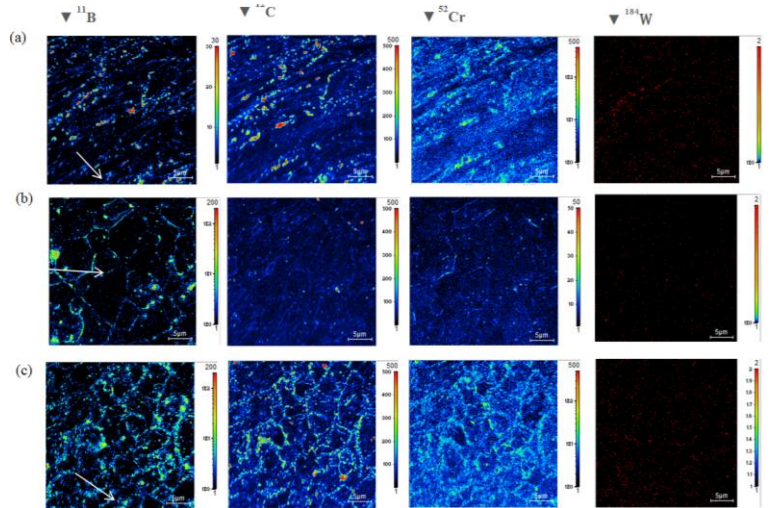
Fig. 1 Nano-SIMS Images of boron, carbon, chromium and tungsten with different intermediate heat treatment conditions: (a) tempered condition, (b) normalized condition, and (c) N&T condition.

All ODF calculations were conducted under the assumption of triclinic sample symmetry – given by the rolling direction (RD), the transverse direction (TD), and the normal direction (ND) of a tube – such that $0^o \leq$ {$\varphi1$, Φ, $\varphi2$} $\leq 90^o$.

The main texture components typical in cold-rolled low-carbon steels in the $\varphi_2 = 45^o$ section of the ODF are shown in Fig. 2 (a). The Bcc metals and alloys tend to form α-fibers and γ-fibers. The α-fibers have the orientation and common <110> crystal axis parallel to the RD, including the orientations {001}<110>, {112}<110> and {111}<110> at ($\varphi1$, Φ, $\varphi2$) = (0°, 0°, 45°), (0°, 35°, 45°) and (0°, 54.7^o, 45°) in the Euler space. The γ-fibers consist of orientations with the {111} crystal axis parallel to the ND, including the orientations {111}<110> and {111}<112> at (φ_1, Φ, φ_2) = (60°, 54.7^o, 45°) and (90°, 54.7^o, 45°) in the Euler space. In addition, the Goss orientation {011}<100> is commonly found at (90°, 90°, 45°) in the Euler space [14].

The ODF outcomes in the $\varphi_2 = 45^o$ section after the different heat treatment conditions are shown in Figs. 2 (b)-(e). In all cases, a dominant texture consisting of α-fibers of {hkl}<110> was noted. On the other hand, γ-fibers weakly indicated a texture consist of the {111}<uvw> component. The characteristic texture changes after the heat treatment can readily be visualized by plotting the orientation density along the most important texture fibers.

The evolution outcomes of α-fibers and γ-fibers through the intensity of the ODF according to the heat treatment used are shown in Fig. 3. The ODF intensity
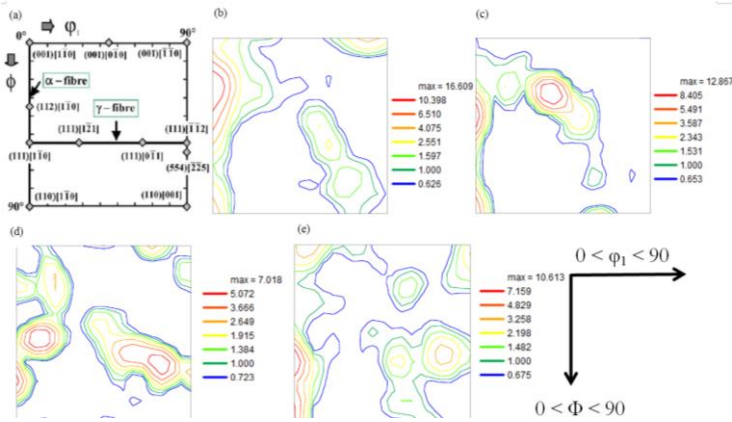
Fig. 2 $\varphi2$ = 45° section of ODF: (a) main orientation, (b) pilgered condition, (c) tempered condition, (d) normalized condition, and (e) N&T condition.

the heat treatment conditions, except for the normalized condition, was dominated by the α-fibers with the maximum between {001}<110> and {111}<110>. Specifically, the α-fibers in the pilgered condition represented the dominant texture of the {113}<110> component with a maximum value of f(g) =16.6 at (0°, 25°, 45°) in the Euler space. However, the normalized condition was dominated by α-fibers with a maximum between {111}<110> and {110}<110>, as presented in Fig. 3 (a).
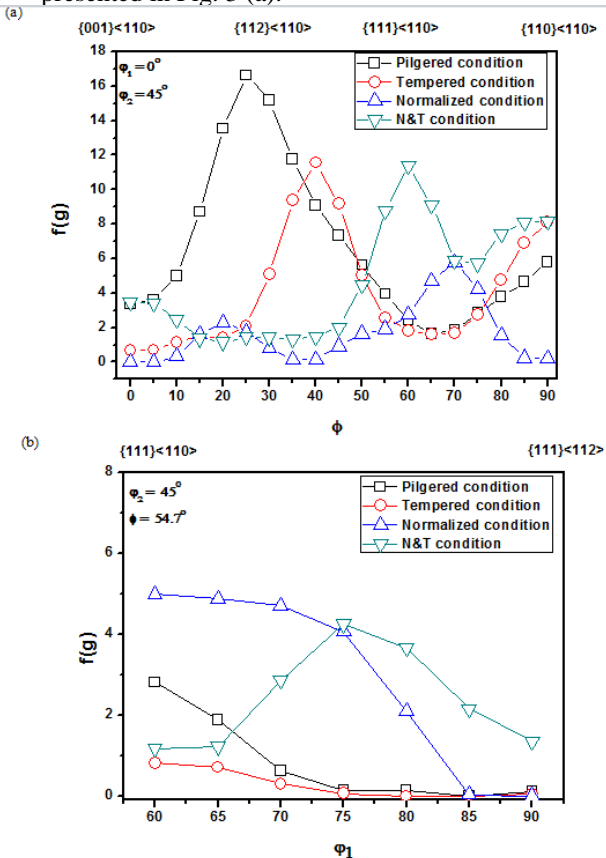
Fig. 3 Evolution of the ODF intensity f(g) with different intermediate heat treatment conditions: (a) α-fiber ($\varphi1$ =0 and $\varphi2$ = 45, constant) and (b) γ-fiber (Φ= 54.7 and $\varphi2$ = 45, constant).

All conditions, expect for the normalized condition, weakly indicated the texture of the {110}<110> component. The ODF intensity levels of the heat treatment conditions were dominated by γ-fibers with a maximum level between {111}<110> and {111}<112>. Specifically, the γ-fibers in the normalized condition and the N&T condition showed a dominant texture of the {111}<110> component with a maximum f(g) =5 at (60°, 54.7^o, 45°) in the Euler space, and presenting a dominant texture {111}<112> component with a maximum value of f(g) =1.3 at (90°, 54.7^o, 45°) in the Euler space, as indicated in Fig. 3 (b).

The main texture component of the α-fiber consists of the {001}<110>, {112}<110>, {111}<110>, and {110}<110> components. The texture {110}<110> component in α-fiber is frequently observed in hot band textures and can remain stable during further rolling. According the Taylor model, the {110}<110> component spreads slightly in the slip direction of {111}<110>. The slip system of the BCC structure consists of a low-index plan (110), (112) and (123) with regard to the critical shear stress for glides; the close-packed directions are <111>. In the BCC structure of the slip system are {110}<111> components, which are related to {111}<110> simply by an exchange of the directions of the glide plane normal and slip vector [5]. The {111}<110> component in the N&T condition was found to have the highest ODF value in α-fibers. The main texture component of the γ-fiber consisted of the {111}<110> and {112}<111> components. The γ-fiber contains two slip systems: {111}<110> and {111}<112>.

The difference between normalized condition and N&T condition is phase transformation, recrystallization. During transformation, although in fact 24 K-S (or 12 N-W) products are expected to be formed, their location can be readily represented by the three Bain products of the cube such as Goss {110}<001>, the rotated Goss {110}<110> and the rotated cube {001}<110>. The texture in the normalized condition and N&T condition is commonly represented in the vicinity of the three bain products component.

The orientation {111}<110> component simultaneously belonging to the α-fiber and γ-fiber remains rather strong after recrystallization. The {111}<110> component in the normalized condition was found to have the highest ODF value. It is well known that the {111}<110> component has the maximum ODF intensity because it is changed by the rotation of {111}<112> around the normal direction [5]

. The {111}<110> component generated by cold working is partially present, and it is judged that the {111}<112> component existing around the normal direction is rotated and formed by the normalizing heat treatment. When the plastic work rate is calculated in the pancake grain interaction mode, the {111}<110> component is reportedly the lowest.

On the other hand, the N&T condition in the γ fiber is the typical recrystallization texture with the {111}<112> component. The formation of {111}<uvw> orientated nuclei in the γ-fiber on the basis of a 30°<111> rotation, as well as the 35°<110> orientation relationship can be explained by a combination of orientated nucleation and grow.

The normalized condition is expected to lead to the most workable texture. However, failures occur under conditions which include normalized tubes with tempering after normalizing the tubes during the drawing process. It is considered that grain boundaries are vulnerable to stress due to excessive segregation of boron at the grain boundaries, as this can lead to failures during the drawing step.

3. Conclusions

1) The segregation of boron occurred at the grain boundary in all intermediate conditions. The different segregation behaviors in the normalized condition and the tempered condition can be explained by the boundary characteristic and by precipitation. When tempering, the amount of boron incorporated into the M23C6 precipitate depends strongly on the location of the precipitate, which is associated with the prior austenite grain boundaries (PAGB). Specifically, the segregation behavior of boron in the N&T condition appears to show both precipitation behavior and non-equilibrium segregation behavior at the grain boundaries.

2) The normalized condition is expected to be the most workable in terms of the texture. However, failures occur under conditions involving normalized tubes which have been tempered after the normalizing tube goes through a drawing process. It is considered that grain boundaries are vulnerable to stress due to the excessive segregation of boron at the grain boundaries, as such a condition will lead to failures during the drawing process.

REFERENCES

[1] J.H. Kim, H.M. Heo, J.H. Baek, S.H. Kim, Evaluation of the mechanical properties of a HT9 fuel cladding tube for a sodium-cooled fast reactor, J. Korean Inst. Met. Mater. 51 (2013) 25–31.

[2] T.K. Kim, S.H. Kim, Study on the cold working process for FM steel cladding tubes, J. Nucl. Mater. 411 (2011) 208–212.

[3] E.H. Jeong, J.H. Kim, S.H. Kim, Y. Do Kim, Influence of B and N on the microstructural characteristics and high-temperature strength of 9Cr-2W steel during an aging treatment, Mater. Sci. Eng. A. 700 (2017) 701–706.

[4] F. Abe, Effect of boron on creep deformation behavior and microstructure evolution in 9Cr steel at 650℃, Int. J. Mater. Res. 99 (2008) 387–394.

[5] H.R. Wenk, Preferred orientation in deformed metals and rocks: An introduction to modern texture analysis, ACADEMIC PRESS, 1985.